Visible-light-sensitive nanoscale Au-ZnO photocatalysts

Ki-Joong Kim[a], Peter B. Kreider[a], Chih-Hung Chang[a,*] Chul-Min Park[b], Ho-Geun Ahn[b]

[a] Oregon Process Innovation Center/Microproduct Breakthrough Institute, School of Chemical, Biological, & Environmental Engineering, Oregon State University, Corvallis, Oregon 97331, United States

[b] Department of Chemical Engineering, Sunchon National University, Suncheon, Jeonnam 540-742, Republic of Korea

*Corresponding author. Tel.: +1 541 737 4791; fax: +1 541 737 4600; E-mail address: chih-hung.chang@oregonstate.edu

Abstract The role of gold nanoparticles supported on ZnO in photocatalytic activity for dye degradation was investigated. To do this, gold nanoparticles supported on ZnO (Au-ZnO) were prepared using a simple co-precipitation method. The prepared nanocatalyst was characterized by high resolution transmission electron microscopy, X-ray diffraction, temperature programmed reduction, X-ray photoelectron spectroscopy, ultraviolet-visible absorption, and photoluminescence. The photocatalytic activity of Au-ZnO was examined by the degradation of methylene blue in aqueous solution using a light source that has more than 95 % (i.e. energy) of emitted photons between 400 and 800 nm. Highly enhanced photocatalytic degradation of methylene blue in air at room temperature was observed from these Au-ZnO nanocatalysts with gold particle size ranging from 2-7 nm, with an average size of 3.8 nm. The observed rate constant for MB degradation on Au-ZnO was 0.0118 min^{-1}, compared to 0.0007 min^{-1} for pure ZnO. Furthermore, the charge transfer pathway for degradation of methylene blue in the Au-ZnO is suggested.

Keywords Gold nanoparticle, Au/ZnO photocatalyst, Visible-light photocatalyst, Methylene blue degradation, Electron transfer pathway.

Introduction

The anatase form of TiO_2 has been extensively investigated in the field of photocatalysis due to its complementary physiochemical properties. ZnO, which is significantly cheaper than TiO_2, is another promising photocatalytic material because it also has a wide, direct energy band gap and a large exciton binding energy (Pauporté and Rathouský. 2007; Zheng et al. 2007; Georgekutty et al. 2008; Hayata et al. 2011). However, the photocatalytic activity of both materials is limited under the sun because the solar spectrum contains only 5-7% of the UV irradiation (Li et al. 2008; Ullah and Dutta 2008). The relatively high recombination rate of generated electron-hole pairs also reduces the efficiency of these photocatalytic materials. Several groups have successfully reduced the recombination rate of excited photoelectron-hole pairs by adding gold nanoparticles (AuNPs) on the surface of ZnO (Wu and Tseng 2006; Lee and Tu 2008; Pawinrat et al. 2009; Wang et al. 2009; Wu et al. 2009; Li et al. 2011; Udawatte et al. 2011). For example, Li et al. (2011) synthesized novel Au-ZnO hybrid nanopryamids with higher photocatalytic efficiency than ZnO nanocrystals. AuNP additions shift the optical absorption into the visible region therefore enable more efficiently utilize solar energy (Chuang and Chen 2009). AuNPs, which could act as a sink for photo-induced charge carriers, also promote interfacial charge-transfer processes (Li et al. 2011; Udawatte et al. 2011). The Fermi energy level of gold is higher than the conduction band energy level of ZnO (Georgekutty et al. 2008; Haldar et al. 2008; Wu et al. 2009). Moreover, oxygen can trap electrons and becomes the active O_2^- species when receiving electrons from the AuNPs surface, thus enhancing the photocatalytic activity (Lee and Tu 2008; Wu et al. 2009; Udawatte et al. 2011). In the present study, AuNPs supported on ZnO was prepared using the co-precipitation method, characterized, and their photocatalytic activity was performed via the degradation of methylene blue (MB) in aqueous solution using a light source that has more than 95 % (i.e. energy) of emitted photons between 400 and 800 nm. Highly enhanced photocatalytic activity for MB degradation in air at room temperature was observed from these nanoscale Au-ZnO photocatalysts for the first time. The charge transfer pathway in the Au-ZnO photocatalyst for the degradation of MB is suggested.

Experimental

Preparation of samples by co-precipitation (CP)

Au-ZnO photocatalysts with 3wt% gold loading using Na_2CO_3 as a precipitating agent was prepared by a simple CP method. An aqueous solution of Na_2CO_3 (EMD Chemicals) solution (1 M, pH = 11.8) was gradually added into the mixture solution of $Zn(NO_3)_2 \cdot 6H_2O$ (Sigma-Aldrich) and $HAuCl_4 \cdot 6H_2O$ (STREM Chemicals) with continuous stirring at 80 ℃. After 1 h, the resulting precipitate was filtered (No. 1, Whatman) and washed with deionized water for 5 times. The paste was dried at room

temperature for 24 h, and was then dried at 100 ℃ for 12 h followed by calcination in static air at 400 ℃ for 3 h. The ZnO was prepared in the same way but without the addition of the gold precursor.

Characterization of samples

The size and dispersion of the AuNPs were observed using high resolution transmission electron microscopy (HRTEM, Titan 80-300, FEI) as well as atomic-resolution high-angle annular dark-field scanning transmission electron microscope (HAADF-STEM) operating at 300 kV in conjunction with energy dispersive spectroscopy (EDS) and with a point resolution of 0.14 nm. The sample was dispersed in ethanol and then dropped onto a copper grid coated with a carbon film. A Histogram of the particle size distribution was obtained by counting at least 126 particles from the STEM images, and the average particle diameter (D_{Au}) was calculated using the formula $D_{Au} = \Sigma di \cdot ni / \Sigma ni$, where ni was the number of particles of diameter di (Bergeret and Gallezot 1997). The crystalline phases were identified by X-ray diffraction (XRD, D8 Discover, Bruker) operating at 40 kV and a current of 40 mA with Cu kα_1 radiation (0.154 nm) in the 2θ scan range from 30° to 70° with a step size of 0.05°. The measured XRD patterns were compared with the JCPDS file. Temperature programmed reduction (TPR) experiments were performed using a commercial TPR apparatus (neo-TPD, Mirae Scientific Instruments). A gaseous mixture of 1%-H_2/in Ar was fed into the reactor at 50 ml/min. The temperature was raised to 500 ℃ at a heating rate of 10 ℃/min. The amount of consumed hydrogen was measured by a thermal conductivity detector. The detailed TPR experimental procedure is given in a previous paper (Kim and Ahn 2009). X-ray photoelectron spectroscopy (XPS) was performed on a ThermoScientific ESCALAB 250 with monochromatized Al Kα X-ray source (1486.6 eV) with 500 μm spot size. The binding energies (BEs) were calibrated using the C 1s signal located at 284.8 eV. The ultraviolet-visible (UV-vis) absorption spectra were measured using a UV-vis-NIR spectrophotometer (V-670, Jasco) in the range of 300-800 nm. The absorption spectra were recorded using 1 cm path length quartz cuvettes. Photoluminescence (PL) spectra were measured using a Xe lamp with an excitation wavelength of 325 nm by a FLS900 spectrometer (Edinburgh Instrument). The BET surface area was measured using N_2 gas adsorption (ASAP 2010, Micromeritics) at -196 ℃.

Photocatalytic activity of methylene blue (MB)

Photocatalytic activity of the prepared photocatalyst was evaluated by the degradation of MB solution. A 500 W Xe lamp (UXL-16B, Ushio) with maximum intensity ($\lambda_{max.}$) at 494 nm was used as a light source. The reactor was set 20 cm away from the output beam. In a typical experiment, 0.1 g of sample was added into 100 mL of 10 mg/L MB solution.

Prior to photocatalytic testing, the solution was stirred for 30 min in darkness in order to reach the adsorption-desorption equilibrium to avoid any error from the initial adsorption effect. Then the solution was irradiated with stirring. At different irradiation time intervals, analytical samples were taken from the reaction suspension, centrifuged at 6,000 rpm for 10 min, filtered through a 0.45 μm Millipore filter to remove the particles, and the filtrate was then analyzed for methylene blue content using a UV-Vis-NIR spectrophotometer (V-670, Jasco) at 664 nm. The rate of degradation was calculated by assuming pseudo-first-order kinetics and hence the rate constant for degradation, k, was obtained from the first-order plot according to the following equation: $\ln(C/C_0) = kt$, where C_0 is the initial absorbance of MB, C is the absorbance of MB after a time (t) and k is the first-order rate constant.

Results and discussion

The morphology of the particles was determined using low and high resolution TEM. Fig. 1a shows the TEM image for the Au-ZnO, and reveals that it has tiny dark spots. HRTEM image and Fourier transform (FT) analyses of the dotted regions in Fig. 1a are also shown in Fig. 1b. The lattice spacing of 0.26 nm corresponds to the (002) plane of the hexagonal ZnO core (JCPDS No. 79-2205) and a lattice spacing of 0.24 nm corresponding to the (111) planes of cubic gold (JCPDS No. 80-0019), respectively. Furthermore, the AuNPs on ZnO appear with a well-ordered hexagonal shape with clear fcc internal structure (Fig. 1c), and the FT image suggest the single crystal structure (inset of Fig. 1c). The size of the particles was determined using HAADF-STEM, which is a powerful technique for determining the structural composition of particles and allows for direct correlation of the optical response with their structural composition. Fig. 1d shows the HADDF-STEM image for the Au-ZnO. Even the smallest gold particles can be seen clearly as bright objects on the dark background and are well dispersed on ZnO. The tiny particles were determined to be monometallic from EDS analysis (Fig. 1e). The X-ray signals of the Au-L1 line were observed at ~2.2, ~9.7 and 11.4 keV. Cu peak at ~8.1 keV appeared as background noise originating from the Cu grid supporting the sample. The results of EDS analysis indicated that the very tiny particles in Fig. 1d correspond to nanosized gold particles supported on ZnO. D_{Au} determined by STEM images is 3.8 nm with a range from 2 to 7 nm (Fig. 1f). These small and relatively uniformly distributed AuNPs even after high temperature calcination suggest sintering resistance which is an indication of strong metal-support interactions (SMSI) (Liu et al. 2012).

The crystalline phases of the ZnO and Au-ZnO were identified by XRD. The XRD patterns confirm that both ZnO and Au-ZnO can only be indexed as the hexagonal phase ZnO (JCPDS No. 79-2205), as shown in Fig. 2. However, the diffraction intensity of Au-ZnO decreases significantly, indicating that some crystal structures might be changed. No peaks of any impurity phases were detected in the XRD pattern. The major peak of gold has to be located at 38.2° for the (111) reflection, however,

the XRD pattern of Au-ZnO show a very weak gold peak at 38.2°. The very low intensity of this gold peak could be due to the following factors: (1) the small gold particle size (< 5 nm), which could cause the diffraction peaks become too broad and be lost in the background of the XRD pattern or (2) the gold (111) peak partially overlaps with the 101 plane ZnO peak.

Fig. 3 shows the UV-vis absorption spectra of ZnO and Au-ZnO. The absorption peak for ZnO and Au-ZnO are centered at 377 nm and 373 nm, respectively, which are attributed to the absorption of microcrystalline ZnO (Anandan and Miyauchi 2011). It can also be clearly observed that the absorption intensity at maximum peaks decreased when AuNPs was added to ZnO. This could be due to an increase in the crystalline disorder in the ZnO crystals with the incorporation of gold, which agrees with the XRD results. The Au-ZnO exhibit an absorption band in the visible region around 560 nm arising from the surface plasmon resonance (SPR) effect of Au (Daniel and Astruc 2004; Wilson 2008; Primo et al. 2011) (inset of Fig. 3) which may cause rapid heating of the AuNPs (Wang et al. 2007). The SPR of AuNPs may also decrease the absorption intensity. The exact position and shape of the surface plasmon band depends on many factors including the dielectric constant of the medium, the particle size, the shape of the particles and the Coulombic charge of the nanoparticle among others (Du et al. 2009). This phenomenon was usually found when AuNPs were combined with semiconductor materials such as CdS, TiO_2, and ZnO to form hybrid nanocrystals (Saunders et al. 2002; Tada et al. 2006), and thus indicated the presence of the hybrid nanostructures in Au-ZnO (Chen et al. 2009). Pure AuNPs typically exhibit an absorption band at 520 nm; however, the absorption band of AuNPs in Au-ZnO is significantly red-shifted by about 40 nm. Yu et al. (2005) also reported specifically that the electron deficiency on the gold surface will shift the absorption band to longer wavelength. The band-gap energies were estimated from a plot of absorbance intensity squared vs band gap energy for ZnO and Au-ZnO, and were ≈ 3.05 eV and ≈ 2.94 eV, respectively.

It is well known that photocatalytic activity is closely related with the recombination rate of photo-excited electrons and holes. PL spectroscopy is a useful method to investigate the efficiency of electron carrier generation, migration, and transfer. Two PL peaks were observed, including a larger emission peak in the UV region at 390 nm and a smaller emission peak in the visible region at 470 nm and 520 nm for both the ZnO and Au-ZnO (Fig. 3). UV peak could be attributed to the recombination of the electrons in the conduction band and the holes in the valence band, while the visible emissions are associated with transitions from the defect-related states, such as oxygen vacancies (O_V), closer to the conduction band edge, to states near the valence band (Djurišić and Leung 2006; Wilson 2008; Lai et al. 2011). Lower PL emission was observed from Au-ZnO nanocatalysts than pure ZnO. The lower PL intensity was a result of lower light absorption and lower radiative recombination rate of electron-hole pairs in the semiconductor (Li et al. 2008; Wu et al. 2009). The intensity of the UV emission in the PL

spectrum is greatly decreased (by a factor of 4.6) when AuNPs are deposited on ZnO. The UV-vis absorption also decreases with the addition of AuNPs, but only by a factor of about 2.1. The transfer of electrons from the ZnO conduction band to the AuNPs leads to non-radiative recombination and a reduction in the intensity of the UV PL peak (Graciani et al. 2008). The visible emission of Au-ZnO was also much lower than that of pure ZnO (by a factor of 6.4). This reduction could be attributed to two possible factors. One is the reduction of O_v via Au atoms filling the O_V, which is the most favored site for Au atoms during the formation of the Au-ZnO interface (Rodriguez et al. 2009; Hou et al. 2012). The other possibility is the absorption of visible emission by AuNPs.

TPR experiments were used to investigate the oxidation state on the AuNPs surface, and the results are shown in Fig. 4. The pure ZnO did not show any strong reduction peaks. When AuNPs are deposited on ZnO however, it was observed that the reduction peaks of gold appeared at 160 ℃ and 245 ℃, respectively. The peak at 160 ℃ is assigned to the reduction of Au^{+3} (Naknam et al. 2009). Au^{+3} is known to be readily reduced (forming Au^{+1} and subsequently Au^0) in reducing atmospheres (Guzman and Gates 2004). The small and broader peak at 245 ℃ could be related with the Au^{+1} to Au^0 reduction or with the reduction of small ionic gold grains encapsulated in partly reduced Au clusters (Sandoval et al. 2007).

To gain more insight into the chemical state and surface compositions of pure ZnO and Au-ZnO, we conducted an XPS analysis. Fig. 5 shows the comparison between the XPS spectra for the C 1s, Zn 2p, O 1s, and Au 4f regions for the ZnO and Au-ZnO. Fig. 5a shows a small C 1s peak in the XPS spectrum of pure ZnO. The C 1s spectrum of Au-ZnO can be deconvoluted into three peaks located at 284.8, 286.2, and 289.2 eV, respectively. The C peak at 284.8 eV can be attributed to the residual carbon from the sample. The carbon peaks at 286.2 and 289.2 eV can be assigned to the carbonyl (C-C/C-OH) and hydroxyl group (C-OH) on the Au-ZnO surface, respectively (Xiao et al. 2012). The larger residual carbon species signal on the Au-ZnO surface than that of the pure ZnO is likely a result of stronger interaction between $HAuCl_4$ as a gold precursor and Na_2CO_3 as a precipitating agent. The Zn 2p spectra of Au-ZnO (Fig. 5b), which consists of two peaks at 1022.5 and 1045.5 eV, are corresponding to Zn $2p_{3/2}$ and Zn $2p_{1/2}$, respectively. The BEs were slightly larger than the corresponding value of zinc in the bulk ZnO, indicating that zinc was in the formal Zn^{2+} valence state within an oxygen-deficient ZnO_{1-x} environment (Peng et al. 2006). The O 1s peak can be fitted into three peaks located at 529.8, 531.0, and 531.9 eV, respectively, as shown in Fig. 5c, indicating three different kinds of oxygen species in both the ZnO and Au-ZnO. The higher oxygen peak at 529.8 eV can be ascribed to the lattice oxygen (O_L) in the wurtzite structure surrounded by the zinc atoms with their full complement of nearest-neighbor O^{2-} ions, and the medium oxygen peak at 531.0 eV is associated with O^{2-} ions in oxygen vacancy (O_V) regions

within the matrix of ZnO. The lower oxygen peak at 531.9 eV is usually attributed to chemisorbed oxygen (O_A) caused by the surface hydroxyl groups, which corresponds to the O-H bonds (Wang et al. 2009; Wu et al. 2011). In comparison with the peak of pure ZnO, the O 1s peak of Au-ZnO shows a slight shift to a higher BE by 0.5 eV. This is likely caused by a charge transfer to the AuNPs. The oxygen species resulting from the O_V of the Au-ZnO shows a decreased intensity compared to that of pure ZnO. It suggests that the O_V were reduced by the addition of AuNPs, which is in good agreement with the PL result. The XPS spectrum of Au 4f partially overlaps with that of Zn 3p spectrum as shown in Fig. 5d. The Au $4f_7$ peak is clearly seen at 83.2 eV although the Au $4f_5$ peak is buried in the strong Zn $3p_3$ peak. In order to see more clearly, the Au 4f spectrum was obtained by subtracting of Zn 3p spectrum from the original data. The fitting procedure was performed by deconvoluting the individual oxidation states contained within the Au 4f peak envelop based on three doublets constructed from a combined Gaussian-Lorentzian line shape. Fig. 5e shows the deconvoluted Au 4f spectrum of Au-ZnO indicates the presence of metallic gold, Au^0 (83.3 and 86.8 eV), which are much lower than that of bulk metallic gold (84.0 and 87.6 eV) (Minicò et al. 2001). This is due to either the larger electronegativity of AuNPs relative to Zn, leading to a charge transfer from the ZnO to the AuNPs at the Au-ZnO interface, or quantum size effect of AuNPs (Do et al. 2010). Furthermore, the Au/ZnO shows two kinds of oxidized gold species (Au^{+1} and Au^{+3}) at 84.8 eV (88.7 eV) and 85.8 eV (90.2 eV), respectively (Qian et al. 2008; Wang et al. 2009). These findings are in good agreement with the TPR results. Recently, Liu et al. (2012) reported SMSI between gold and ZnO nanorods based on the results of structural and spectroscopic characterization. The Au/ZnO catalyst shows electron transfer between gold and ZnO support. The hexagonal shape of AuNPs with facets (Fig. 1b) which has been reported in Au-ZnO (Radnik et al. 2003; Claus 2005), exhibiting surfaces with large facets indicate a fairly strong interaction between gold and ZnO (Radnik et al. 2003; Donkova et al. 2011). We believe that the existence of oxidic Au species might be a result of SMSI between gold and ZnO. The total ratio of XPS intensity ($I_{Au(I)+Au(III)}/I_{Au(0)}$) for the gold species on Au-ZnO was estimated to be 0.77. UV-vis absorption, TPR, and XPS results all support that there is a large fraction of oxidic Au species in the AuNPs. This large fraction of oxidic Au species in Au-ZnO catalysts could be important for high photocatalytic activity under visible light.

The photocatalytic performance of Au-ZnO was tested in terms of the degradation of MB using simulated sunlight. Fig. 6 shows the UV-vis absorption spectra of MB in the presence of 0.1 g of suspended Au-ZnO at varying irradiation times. The peak at 664 nm is attributed to the absorbance of n $\rightarrow \pi^*$ transition in MB (Heger et al. 2005). It can be clearly seen that the concentration of MB decreased dramatically as the irradiation time increased. Fig. 7 shows the comparative study of MB degradation under irradiation for pure MB solution, MB with suspended ZnO, and MB with suspended Au/ZnO. The

spectrum of the xenon lamp has an emission that peaks at 494 nm ($\lambda_{max.}$ = 494 nm) and has more than 95 % of total energy within the visible range between 400 and 800 nm, which approaches real sunlight. Before reaction, C/C_0 of ZnO and Au/ZnO for MB are shown at a value 0.66 and 0.67, respectively. This preliminary decrease of the MB concentration is due to the initial amount adsorbed onto the samples when stirred in the dark. For reference, the BET surface area of ZnO and Au-ZnO were 24.5 and 22.5 $m^2 g^{-1}$, respectively.

It was observed that MB cannot be easily degraded within 240 min by photolysis. Pure ZnO shows poor photocatalytic activity for MB degradation in spite of higher UV-vis absorption. Complete degradation of MB on Au/ZnO was observed within 240 min. Several studies have reported significant photocatalytic activity for pure ZnO for MB degradation when a UV light source is used (Pawinrat et al. 2009; Chang et al. 2011; Li et al. 2011). Pure ZnO, however has very little photocatalytic activity under visible light irradiation (Ziao et al. 2007; Wang et al. 2009; Zhang and Zeng 2012).

The photocatalytic degradation of MB is greatly enhanced when AuNPs are dispersed on the ZnO surface. Although the UV-vis absorption decreased with the addition of AuNPs, their presence on the surface of ZnO improves the photocatalytic activity. It is generally accepted that the excited photoelectrons from the ZnO conduction band can quickly and easily transfer to the AuNPs surface which allows for efficient separation of photoelectron (e^-) and hole (h^+) pairs (Wang et al. 2009; Subramanian 2003). The kinetics of photocatalytic degradation was investigated. First-order degradation rate constants, obtained by plotting the natural logarithm of the absorbance vs irradiation time are shown in Fig. 8. The kinetic data of the MB photocatalytic degradation fit well to the pseudo-first-order reaction kinetic model (R^2 =0.998). The rate constants (k) of the ZnO and the Au-ZnO for the degradation of MB of 10 mg L^{-1} were found to be 0.0007 min^{-1} and 0.0118 min^{-1}, respectively, and k value of the Au/ZnO was ca. 17 times higher than that of pure ZnO. This enhancement factor (17 times) is much more pronounced than previously reported result (1.4 times) that used UV excitation light source (Pawinrat et al. 2009).

We suggest a possible mechanism for the degradation of MB on the Au-ZnO photocatalyst under simulated sunlight. The proposed mechanism is illustrated in Fig. 9. Charge generation and separation occurred within Au-ZnO nanocatalysts under light irradiation. The excited photoelectrons were transferred to the adsorbed O_2. It should be noted that O_2 adsorption proceeds directly on AuNPs surface (Valden et al. 1998; Schubert et al. 2001). This leads to the highly oxidizing peroxy or superoxy species (O_2^-), whereas the h^+ can be easily trapped by electronic donors, such as OH^-, to further oxidize organic pollutants (Wang et al. 2009). Therefore, allows for an effective separation of e^- and h^+, thus significantly enhancing the photocatalytic activityfor MB degradation.

Conclusions

Au-ZnO nanocatalysts were prepared by the simple CP method. These Au-ZnO nanocatalysts are highly sensitive to visible light. The recombination rate of the photo-exited electron-hole pairs was significantly reduced by the addition of AuNPs because photoelectrons from the ZnO conduction band can quickly and easily transfer to the AuNPs surface which allows for efficient charge carrier separation. This leads to highly enhanced photocatalytic efficiency for MB degradation under a light source that has more than 95 % (i.e. energy) of emitted photons between 400 and 800 nm in air at room temperature. The enhancement factor is an order of magnitude higher (17 times) than previously reported values using a UV light source.

Acknowledgement

This work was financially supported by the Oregon Nanoscience and Micro- technologies Institute (ONAMI) and Oregon Built Environment & Sustainable Technologies (Oregon BEST) center. The authors would like to thank Paravee Vas-Umnuay for her help with the solar simulator set-up. The authors also thank Won-Ju Ahn at Sunchon National University for conducting the TPR experiments and Dr. Tomas Novet at Voxtel for the Photoluminescence measurements. We are thankful to Dr. Stephen Golledge and Joshua Raznik at CAMCOR, University of Oregon, for valuable assistance in obtaining, analyzing and interpreting XPS and HRTEM data.

References

Anandan S, Miyauchi M (2011) Ce-doped ZnO ($Ce_xZn_{1-x}O$) becomes an efficient visible-light-sensitive photocatalyst by co-catalyst (Cu^{2+}) grafting. Phys Chem Chem Phys 13(33):14937-14945

Bergeret G, Gallezot P (1997) Handbook of heterogeneous catalysis, In: Ertl G, Knozinger H (ed) VCH, Weinheim, pp 439-462

Chang H, Nikolov J, Kim S-K, Jang HD, Lim S, Kim D-J (2011) Preparation and characterization of vanadium-doped ZnO nanoparticles for environmental application. J Nanosci Nanotechnol 11(1):681-685

Chen B, Zhang H, Du N, Li D, Ma X, Yang D (2009) Hybrid nanostructures of Au nanocrystals and ZnO nanorods: layer-by-layer assembly and tunable blue-shift band gap emission. Mater Res Bull 44(4):889-892

Chuang H-Y, Chen D-H (2009) Fabrication and photocatalytic activities in visible and UV light regions of $Ag@TiO_2$ and $NiAg@TiO_2$ nanoparticles. Nanotechnology 20(10):105704

Claus P (2005) Heterogeneously catalysed hydrogenation using gold catalysts. Appl Catal A: Gen 291(1-2):222-229

Daniel MC, Astruc D (2004) Gold nanoparticles: assembly, supramolecular chemistry, quantum-size-

related properties, and applications toward biology, catalysis, and nanotechnology. Chem Rev 104(1):293-346

Djurišić AB, Leung YH (2006) Optical properties of ZnO nanostructures. Small 2(8-9):944-961

Donkova B, Vasileva P, Nihtianova D, Velichkova N, Stefanov P, Mehandjiev D (2011) Synthesis, characterization, and catalytic application of Au/ZnO nanocomposites prepared by coprecipitation. J Mater Sci 46(22):7134-7143

Do Y, Choi J-S, Kim SK, Sohn Y (2010) The interfacial nature of TiO_2 and ZnO nanoparticles modified by gold nanoparticles. Bull Korean Chem Soc 31(8):2170-217

Du L, Furube A, Yamamoto K, Hara K, Katoh R, Tachiya M (2009) Plasmon-induced charge separation and recombination dynamics in gold-TiO_2 nanoparticle systems: dependence on TiO_2 particle size. J Phys Chem C 113(16):6454-6462

Georgekutty R, Seery MK, Pillai SC (2008) A highly efficient Ag-ZnO photocatalyst: synthesis, properties, and mechanism. J Phys Chem C 112(35):13563-13570

Graciani J, Nambu A, Evans J, Rodriguez JA, Sanz JF (2008) Au ↔ N synergy and N-doping of metal oxide-based photocatalysts. J Am Chem Soc 130(36):12056-12063

Guzman J, Gates BC (2004) Catalysis by supported gold: correlation between catalytic activity for CO oxidation and oxidation states of gold. J Am Chem Soc 126(9):2672-2673

Haldar KK, Sen T, Patra A (2008) Au@ZnO core-shell nanoparticles are efficient energy acceptors with organic dye donors. J Phys Chem C 112(31):11650-11656

Hayata K, Gondalb MA, Khaleda MM, Ahmedc S, Shemsi AM (2011) Nano ZnO synthesis by modified sol gel method and its application in heterogeneous photocatalytic removal of phenol from water. Appl Catal A: Gen 393(1-2):122-129

Heger D, Jirkovský J, Klán P (2005) Aggregation of methylene blue in frozen aqueous solutions studied by absorption spectroscopy. J Phys Chem A 109(30):6702-6709

Hou X, Wang L, He G, Ha J (2012) Synthesis, optical and electrochemical properties of ZnO nanorod hybrids loaded with high-density gold nanoparticles. Cryst Eng Comm 14(16):5158-5162

Kim K-J, Ahn H-G (2009) Complete oxidation of toluene over bimetallic Pt-Au catalysts supported on ZnO/Al_2O_3. Appl Catal B: Environ 91(1-2):308-318

Lai JJ, Lin YJ, Chen YH, Chang HC, Liu CJ, Zou YY, Shih YT, Wang MC (2011) Effects of Na content on the luminescence behavior, conduction type, and crystal structure of Na-doped ZnO films. J Appl Phys 110(1):013704

Lee MK, Tu HF (2008) Au-ZnO and Pt-ZnO films prepared by electrodeposition as photocatalysts. J Electrochem Soc 155(12):D758-D762

Li H, Liu E.-T, Chan FYF, Lu Z, Chen R (2011) Fabrication of ordered flower-like ZnO nanostructures by

a microwave and ultrasonic combined technique and their enhanced photocatalytic activity. Mater Lett 35(23-24):3440-3443

Li P, Wei Z, Wu T, Peng Q, Li Y (2011) Au-ZnO hybrid nanopyramids and their photocatalytic properties. J Am Chem Soc 133(15):5660-5663

Liu X, Liu M-H, Luo Y-C, Mou C-Y, Lin SD, Cheng H, Chen J-M, Lee J-F, Lin T-S (2012) Strong metal-support interactions between gold nanoparticles and ZnO nanorods in CO oxidation. J Am Chem Soc 134(24):10251-10258

Li Y, Zhang H, Guo Z, Han J, Zhao X, Zhao Q, Kim SJ (2008) Highly efficient visible-light-induced photocatalytic activity of nanostructured AgI/TiO_2 photocatalyst. Langmuir 24(15):8351-8357

Minicò S, Scirè S, Crisafulli C, Galvagno S (2001) Influence of catalyst pretreatments on volatile organic compounds oxidation over gold/iron oxide. Appl Catal B: Environ 34(4):277-285

Naknam P, Luengnaruemitchai A, Wongkasemjit S (2009) Au/ZnO and Au/ZnO-Fe_2O_3 prepared by deposition-precipitation and their activity in the preferential oxidation of CO. Energy Fuels 23(10):5084-5091

Pauporté T, Rathouský J (2007) Electrodeposited mesoporous ZnO thin films as efficient photocatalysts for the degradation of dye pollutants. J Phys Chem C 111(21):7639-7644

Pawinrat P, Mekasuwandumrong O, Panpranot J (2009) Synthesis of Au-ZnO and Pt-ZnO nanocomposites by one-step flame spray pyrolysis and its application for photocatalytic degradation of dyes. Catal Commun 10(10):1380-1385

Peng Y-Y, Hsieh T-E, Hsu C-H (2006) White-light emitting ZnO-SiO_2 nanocomposite thin films prepared by the target-attached sputtering method. Nanotechnology 17(1):174-180

Primo A, Corma A, García H (2011) Titania supported gold nanoparticles as photocatalyst. Phys Chem Chem Phys 13(3):886-910

Qian K, Huang W, Fang J, Lv S, He B, Jiang Z, Wei S (2008) Low-temperature CO oxidation over Au/ZnO/SiO_2 catalysts: some mechanism insights. J Catal 255(2):269-278

Radnik J, Mohr C, Claus P (2003) On the origin of binding energy shifts of core levels of supported gold nanoparticles and dependence of pretreatment and material synthesis. Phys Chem Chem Phys 5(1):172-177

Rodriguez JA, Evans J, Graciani J, Park J-B, Liu P, Hrbek J, Sanz JF (2009) High water-gas shift activity in TiO_2(110) supported Cu and Au nanoparticles: role of the oxide and metal particle size. J Phys Chem.C 113(17):7364-7370

Sandoval A, Gomez-Cortes A, Zanella R, Dıaz G, Saniger JM (2007) Gold nanoparticles: support effects for the WGS reaction. J Mol Catal A: Chem 278(1-2):200-208

Saunders AE, Popov I, Banin U (2002) Synthesis of hybrid CdS-Au colloidal nanostructures. J Phys

Chem B 110(50):25421-25429

Subramanian V, Wolf EE, Kamat PV (2003) Green emission to probe photoinduced charging events in ZnO-Au nanoparticles. charge distribution and Fermi-level equilibration. J Phys Chem B 107(30):7479-7485

Schubert MM, Hackenberg S, van Veen AC, Muhler M, Plzak V, Behm RJ (2001) CO Oxidation over supported gold catalysts-"inert" and "active" support materials and their role for the oxygen supply during reaction. J Catal 197(1):113-122

Tada H, Mitsui T, Kiyonaga T, Akita T, Tanaka K (2006) All-solid-state Z-scheme in CdS-Au-TiO_2 three-component nanojunction system. Nat Mater 5(10):782-786

Udawatte N, Lee M, Kim J, Lee D (2011) Well-defined Au/ZnO nanoparticle composites exhibiting enhanced photocatalytic activities. ACS Appl Mater Interfaces 3(11):4531-4538

Ullah R, Dutta J (2008) Photocatalytic degradation of organic dyes with manganese-doped ZnO nanoparticles. J Hazard Mater 156(1-3):194-200

Valden M, Pak S, Lai X, Goodman DW (1998) Structure sensitivity of CO oxidation over model Au/TiO_2 catalysts. Catal Lett 56(1):7-10

Wang LC, Liu Q, Huang XS, Liu YM, Cao Y, Fan KN (2009) Gold nanoparticles supported on manganese oxides for low-temperature CO oxidation. Appl Catal B: Environ 88(1-2):204-212

Wang Q, Geng B, Wang S (2009) ZnO/Au hybrid nanoarchitectures: wet-chemical synthesis and structurally enhanced photocatalytic performance. Environ Sci Technol 43(23):8968-8973

Wang X, Kong X, Yu Y, Zhang H (2007) Synthesis and characterization of water-soluble and bifunctional ZnO-Au nanocomposites. J Phys Chem C 111(10):3836-3841

Wilson R (2008) The use of gold nanoparticles in diagnostics and detection. Chem Soc Rev 37(9):2028-2045

Wu JJ, Tseng CH (2006) Photocatalytic properties of nc-Au/ZnO nanorod composites. Appl Catal B: Environ 66(1-2):51-57

Wu JM, Fang C-W, Lee LT, Yeh H-H, Lin Y-H, Yeh P-H, Tsai L-N, Lin L-J (2011) Photoresponsive and ultraviolet to visible-light range photocatalytic properties of ZnO:Sb nanowires. J Electrochem Soc 158(1):K6-K10

Wu Y, Liu H, Zhang J, Chen F (2009) Enhanced photocatalytic activity of nitrogen-doped titania by deposited with gold. J Phys Chem C 113(33):14689-14695

Xiao F, Wang F, Fu X, Zheng Y (2012) A green and facile self-assembly preparation of gold nanoparticles/ZnO nanocomposite for photocatalytic and photoelectrochemical applications. J Mater Chem 22(7):2868-2877

Xiao Q, Zhang J, Xiao C, Tan X (2007) Photocatalytic decolorization of methylene blue over $Zn_{1-x}Co_xO$

under visible light irradiation. Mater Sci Eng B 142(2-3):121-125

Yu H, Chen M, Rice PM, Wang SX, White RL, Sun S (2005) Dumbbell-like bifunctional Au-Fe_3O_4 nanoparticles. Nano lett 5(2):379-382

Zhang D, Zeng F (2012) Visible light-activated cadmium-doped ZnO nanostructured photocatalyst for the treatment of methylene blue dye. J Mater Sci 47(5):2155-2161

Zheng Y, Chen C, Zhan Y, Lin X, Zheng Q, Wei K, Zhu J, Zhu Y (2007) Luminescence and photocatalytic activity of ZnO nanocrystals: correlation between structure and property. Inorg Chem 46(16):6675-6682

Figure captions

Fig. 1. (a) TEM image, (b) HRTEM image for dotted line in Fig. 1a (insert of FT image), (c) AuNP on ZnO with single crystal structure (insert of FT image), (d) HADDF-STEM image (e) EDS spectra from particles indicated by arrow 1 and 2 in Fig. 1d, and (f) distribution of AuNPs in the Au-ZnO.

Fig. 2. XRD patterns of ZnO and Au-ZnO (insert of magnified XRD pattern for Au (111) plane).

Fig. 3. UV-vis absorption spectra (solid line) and Room-temperature PL spectra (dotted line) of ZnO and Au-ZnO (insert of magnified SPR effect).

Fig. 4. TPR profiles of ZnO and Au-ZnO.

Fig. 5. XPS spectra in the (a) C 1s, (b) Zn 2p, (c) O 1s, (d) Zn 3p and Au 4f, and (e) Au 4f regions for the ZnO and Au-ZnO photocatalysts. Au 4f XPS spectrum of Au-ZnO after subtracting the Zn 3p from the original XPS data.

Fig. 6. Absorption spectra of MB solution (10 mg L^{-1}) with irradiation time in the presence of Au-ZnO (0.1 g) under simulated sunlight (xenon lamp, $\lambda_{max.} = 494$ nm).

Fig. 7. Photocatalytic activities under simulated sunlight of without sample, ZnO, and Au-ZnO. The wavelength of simulated sunlight ($\lambda_{max.}$ = 494 nm) was recorded by USB 2000 fiber optic spectrometer (Ocean Optics).

Fig. 8. A plot of ln (C/C_0) vs irradiation time under simulated sunlight of without sample, ZnO, and Au-ZnO.

Fig. 9. Proposed mechanism for MB degradation over Au-ZnO photocatalyst. Electron-transfer pathway in ZnO (solid line) and Au-ZnO (dotted line). V_o is denotes oxygen vacancy.

Figures

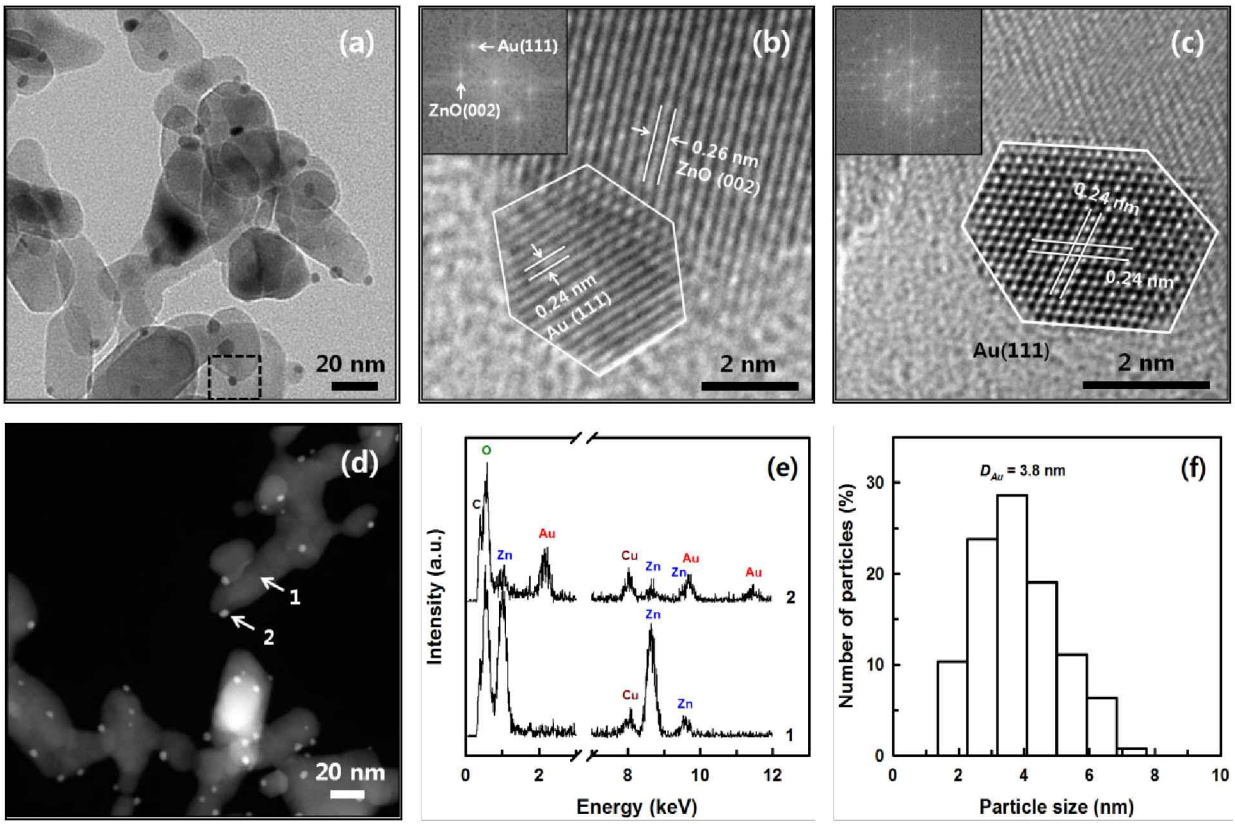

Fig. 1. (a) TEM image, (b) HRTEM image for dotted line in Fig. 1a (insert of FT image), (c) AuNP on ZnO with single crystal structure (insert of FT image), (d) HADDF-STEM image (e) EDS spectra from particles indicated by arrow 1 and 2 in Fig. 1d, and (f) distribution of AuNPs in the Au-ZnO.

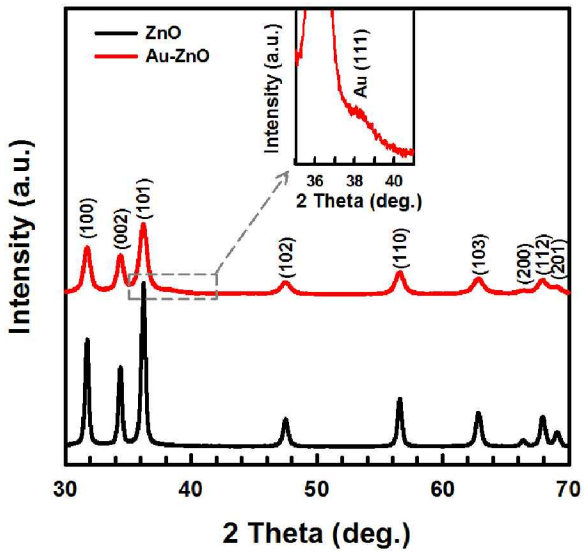

Fig. 2. XRD patterns of ZnO and Au-ZnO (insert of magnified XRD pattern for Au (111) plane).

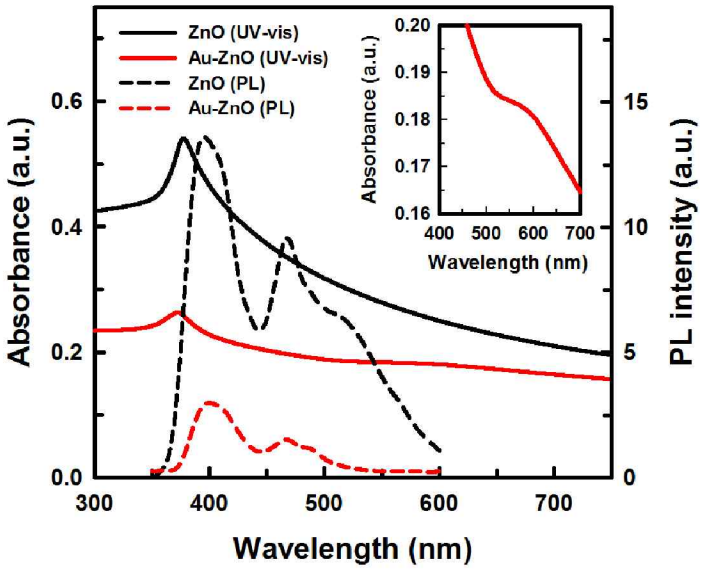

Fig. 3. UV-vis absorption spectra (solid line) and Room-temperature PL spectra (dotted line) of ZnO and Au-ZnO (insert of magnified SPR effect).

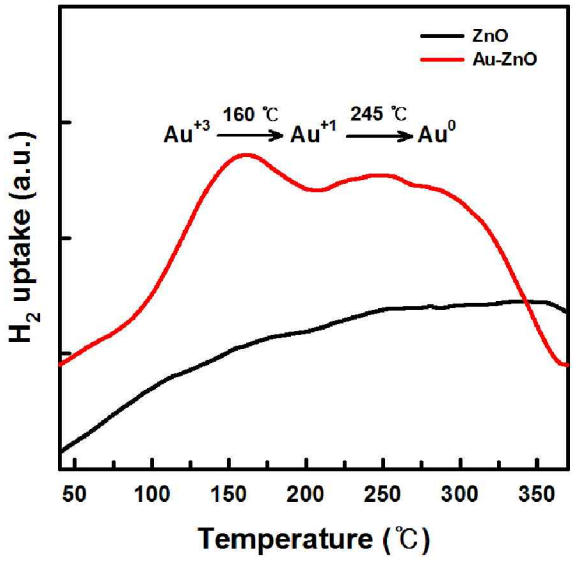

Fig. 4. TPR profiles of ZnO and Au-ZnO.

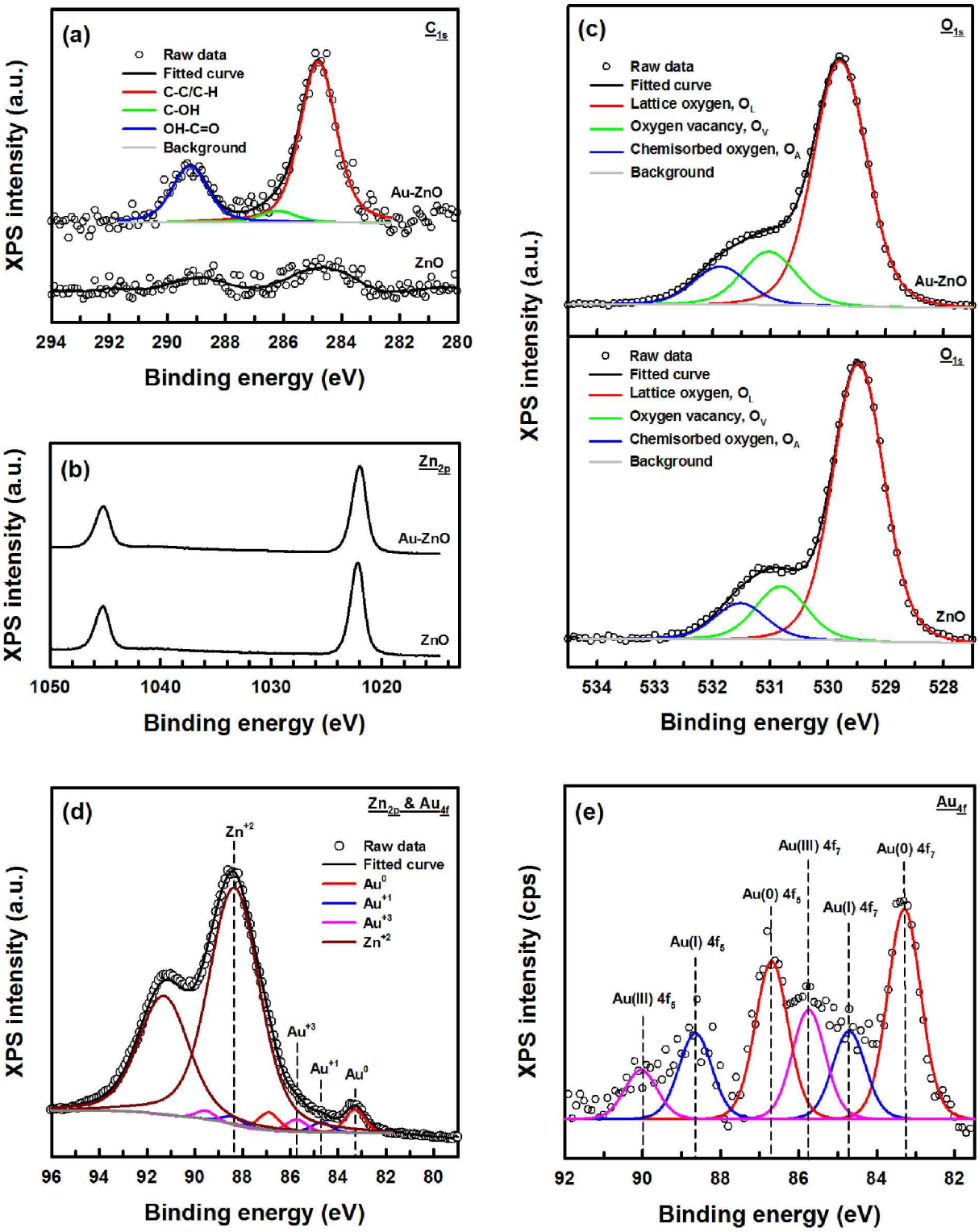

Fig. 5. XPS spectra in the (a) C 1s, (b) Zn 2p, (c) O 1s, (d) Zn 3p and Au 4f, and (e) Au 4f regions for the ZnO and Au-ZnO photocatalysts. Au 4f XPS spectrum of Au-ZnO after subtracting the Zn 3p from the original XPS data.

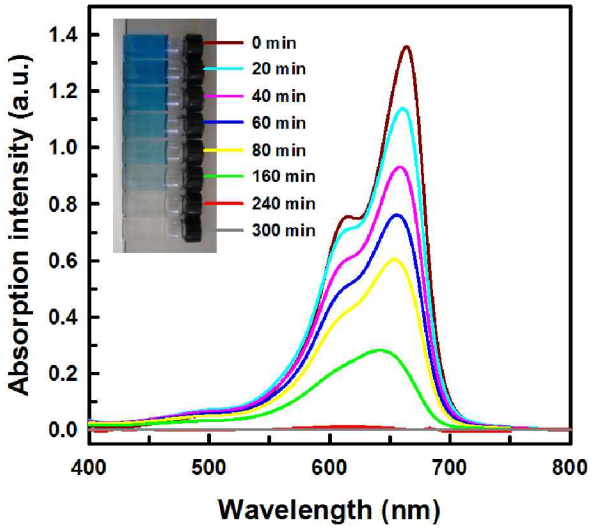

Fig. 6. Absorption spectra of MB solution (10 mg L^{-1}) with irradiation time in the presence of Au-ZnO (0.1 g) under simulated sunlight (xenon lamp, $\lambda_{max.}$ = 494 nm).

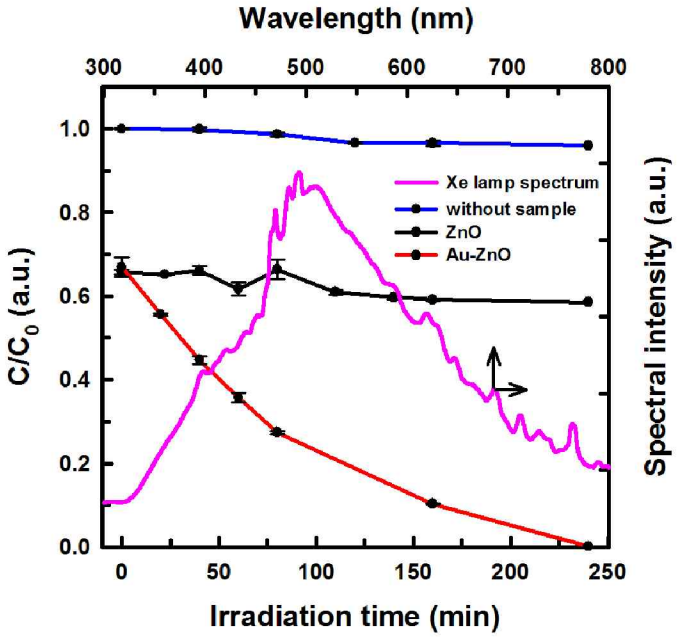

Fig. 7. Photocatalytic activities under simulated sunlight of without sample, ZnO, and Au-ZnO. The wavelength of simulated sunlight (>320 nm, $\lambda_{max.}$ = 494 nm) was recorded by USB 2000 fiber optic spectrometer (Ocean Optics).

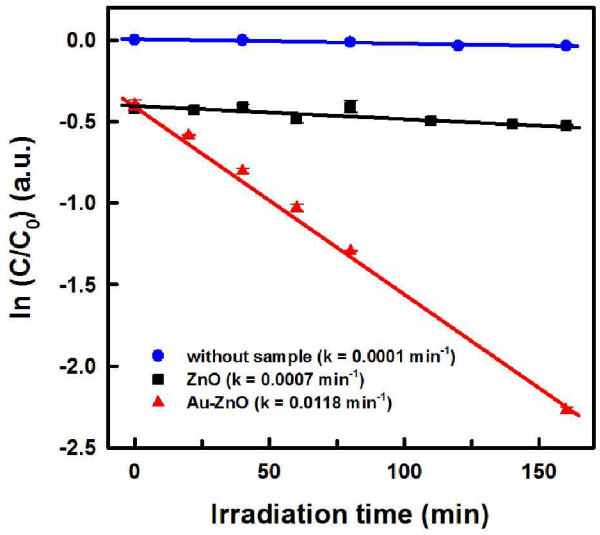

Fig. 8. A plot of ln (C/C_0) vs irradiation time under simulated sunlight of without sample, ZnO, and Au-ZnO.

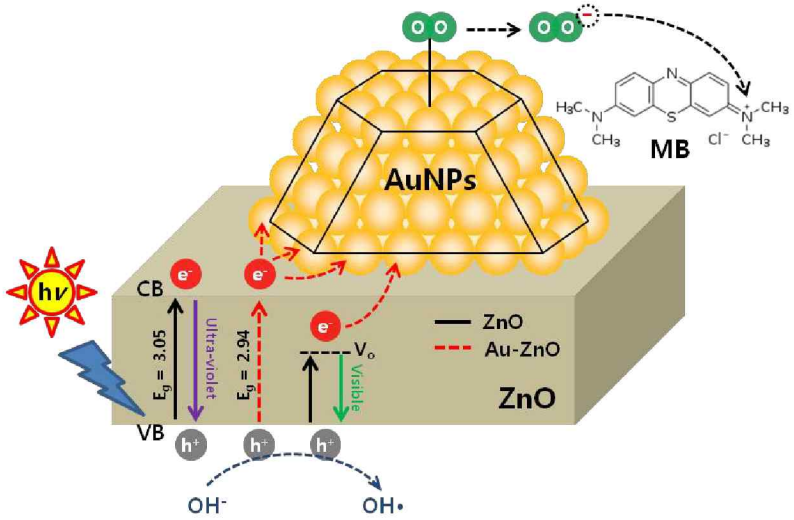

Fig. 9. Proposed mechanism for MB degradation over Au-ZnO photocatalyst. Electron-transfer pathway in ZnO (solid line) and Au-ZnO (dotted line). V_o is denotes oxygen vacancy.